Origin of Improvement in Mechanical Quality Factor in Acceptor-Doped Relaxor-Based Ferroelectric Single Crystals

Limei Zheng,[1] Liya Yang,[1] Yanran Li,[1] Xiaoyan Lu,[2] Da Huo,[1] Weiming Lü,[1,*] Rui Zhang,[1] Bin Yang,[1] and Wenwu Cao[1,3,†]

[1]*Condensed Matter Science and Technology Institute and Department of Physics, Harbin Institute of Technology, Harbin 150080, China*

[2]*School of Civil Engineering, Harbin Institute of Technology, Harbin 150001, China*

[3]*Department of Mathematics and Materials Research Institute, The Pennsylvania State University, University Park, Pennsylvania 16802, USA*

(Received 26 November 2017; revised manuscript received 27 March 2018; published 19 June 2018)

The mechanical quality factor Q_m in ferroelectric materials can be improved via acceptor doping to extend their application in high-power devices. It is generally believed that the improvement of Q_m originates from the pinning effect of internal bias. However, the contributions from restricted spontaneous polarization (P_S) rotation and clamped domain-wall motion are difficult to separate, leading to some ambiguities about the effect of doping. We report on a strong anisotropic pinning effect in Mn-doped $0.27Pb(In_{1/2}Nb_{1/2})O_3$-$0.46Pb(Mg_{1/3}Nb_{2/3})O_3$-$0.27PbTiO_3$ single crystals and investigate the related mechanism. We observe that the domain-wall motion is not clamped by the internal bias but are strongly pinned by charged defects at the charged domain walls, whereas the P_S rotation is suppressed by the internal bias. We also confirm that the enhancement of longitudinal factor Q_{33} is attributed mainly to the restricted polarization rotation, whereas the enhancement of shear factor Q_{15} is ascribed to both the restricted polarization rotation and the clamped domain-wall motion. Our results reveal the fundamental mechanism of the acceptor doping effects in relaxor-based ferroelectric materials, and they also provide important design principles to achieve high-Q_m piezoelectric materials to satisfy the demands of high-power electromechanical devices.

DOI: 10.1103/PhysRevApplied.9.064028

I. INTRODUCTION

The doping of relaxor-based ferroelectric single crystals, from binary $(1-x)Pb(Mg_{1/3}Nb_{2/3})O_3$-$xPbTiO_3$ (PMN-xPT) to ternary $Pb(In_{1/2}Nb_{1/2})O_3$-$Pb(Mg_{1/3}Nb_{2/3})O_3$-$xPbTiO_3$ (PIN-PMN-xPT) systems, has substantially increased the coercive field E_C and the rhombohedral-to-tetragonal phase transition temperature $T_{R\text{-}T}$ [1–6]. However, these materials generally have a very low mechanical quality factor Q_m, which limits their applications in high-power imaging transducers and sensors. The subsequent objective is to improve these materials to achieve a higher mechanical quality factor Q_m for applications in high-power electromechanical devices, such as sonar projectors and piezoelectric transformers, where Q_m is the inverse of the mechanical loss.

Similar to other properties of ferroelectrics, mechanical loss can be divided into intrinsic and extrinsic parts. The intrinsic part is associated with spontaneous polarization (P_S) rotation with respect to the external field, and the extrinsic part mainly originates from the movement of the domain wall [7]. Both are lossy processes. Thus, there are two ways to improve Q_m: by restricting P_S rotation and by clamping domain-wall motion [8]. It is known that Q_m can be enhanced via acceptor ion doping, which introduces an internal bias (abbreviated as E_i). It is commonly believed that both P_S rotation and domain-wall motion are pinned by the internal bias [9–12]. However, the mechanism of pinning of the P_S rotation and domain-wall motion and their respective quantified impact on the enhancement of Q_m are still unclear. The lack of fundamental understanding hinders the optimization of high-Q_m piezoelectric materials. It was demonstrated recently that the improvement of Q_m is strongly anisotropic in acceptor-doped relaxor PT-based single crystals [9,10], which indicates that the pinning effect may be anisotropic. In order to elucidate the underlying mechanism of anisotropic enhancement of Q_m, a quantitative study on the pinning effect of domain-wall dynamics and polarization rotation is required, and the physical origin of this pinning effect should also be explored.

In this work, we quantitatively estimate the domain-wall mobility and P_S rotation in different modes (under electric

*Corresponding author.
weiminglv@hit.edu.cn
†Corresponding author.
dzk@psu.edu

fields parallel to and perpendicular to the poling direction, abbreviated as $E_{||}$ and $E_{\perp}$, respectively) in Mn-doped PIN-PMN-xPT single crystals, with the purpose of further understanding the pinning effect and the mechanism of Q_m improvement in acceptor-ion-doped ferroelectrics.

II. EXPERIMENTAL DETAILS

A. Sample preparation

In order to reduce the influence of the morphotropic phase boundary (MPB) and the polymorphic phase transition, a relaxor-based ferroelectric crystal $0.27Pb(In_{1/2}Nb_{1/2})O_3$-$0.46Pb(Mg_{1/3}Nb_{2/3})O_3$-$0.27PbTiO_3$ doped with 1.5 mol % Mn (PIN-PMN-0.27PT:Mn) is chosen, which is in the pure rhombohedral (R) phase, sufficiently far away from the MPB, and with a rhombohedral-tetragonal phase transition temperature $T_{R\text{-}T}$ (approximately 120 °C) that is well above room temperature [9]. The corresponding properties of crystals without Mn doping, PIN-PMN-0.27PT (also far away from the MPB with a $T_{R\text{-}T}$ value of approximately 116 °C), are also measured for the sake of comparison [11]. Both PIN-PMN-0.27PT and PIN-PMN-0.27PT:Mn crystals (TRS Technologies, State College, Pennsylvania) are fabricated using the modified Bridgman method. All of the samples are oriented using the real-time Laue x-ray diffraction method with an accuracy of ±0.5°. After cutting and polishing, all of the samples are annealed at 600 °C for 1 h to eliminate the stresses generated during preparation. Vacuum-sputtered gold is applied to the desired surfaces as electrodes. The PIN-PMN-0.27PT and PIN-MN-0.27PT:Mn crystals are poled along $[001]_C$ under dc fields of 10 kV cm^{-1} and 12 kV cm^{-1}, respectively, for 15 min at 25 °C.

B. Property characterization

All of the samples are sufficiently aged for three days after being poled before the electrical measurements are carried out. The rhombohedral-tetragonal phase transition temperature $T_{R\text{-}T}$ is determined from the dielectric constant ε_{33} versus temperature curve, which is measured using an HP4284A *LCR* meter connected to a computer-controlled temperature chamber. Polarization–electric-field loops (P-E loops) are measured using a Precision Premier II tester (Radiant Technologies, Albuquerque). A triangular waveform pulse with the frequency of 1 Hz is used for the P-E measurements. Before the measurement, one cycle of the proposed pulse is applied, followed by a delay of 1 s, and the measured pulse is then applied. The schematic for the ac signal can be seen in Fig. S2 of the Supplemental Material [8].

For the P-E loops and dielectric Rayleigh behavior measured under $E_{\perp}$, electrodes are removed after poling and reelectroded on the $(100)_C/(010)_C$ surfaces. In Rayleigh measurements, an ac E field with the amplitude E_0 ranging from 0.3 kV cm^{-1} to 1.5 kV cm^{-1} is applied on the sample with an increment of 0.1 kV cm^{-1} to obtain P-E loops under subswitching conditions. The mechanical quality factor Q_m is measured using the 3-dB method at the resonance frequency.

C. Domain observation

The domain structures are observed using polarizing light microscopy (Zeiss Axioskop 40) with crossed polarizer-analyzer pairs and piezoresponse force microscopy (Asylum Research, Cypher ES). For domain observations, the two $(001)_C$ surfaces of the samples are polished to obtain optical quality. Silver paste is applied on the two $(001)_C$ surfaces as electrodes. After being poled, silver electrodes are removed with acetone for domain observation.

III. RESULTS AND ANALYSES

The actual concentration of Mn in a PIN-PMN-0.27PT:Mn single crystal determined using x-ray fluorescence spectrometry is 0.75%, which is lower than the nominal content of 1.5%. For the rhombohedral phase, eight possible spontaneous polarization (P_S) directions along the $\langle 111\rangle_C$ family exist [8]. After poling along $[001]_C$, only four upward P_S directions remain and the domain structure becomes a "4R" multidomain state [8].

A. Quantitative determination of domain-wall mobility

Domain-wall mobility in a ferroelectric material is closely related to the extrinsic dielectric and piezoelectric contributions. In this work, Rayleigh law (detailed information about Rayleigh law can be found in Sec. B of the Supplemental Material [8]) is adopted to extract the extrinsic dielectric contribution, and the domain-wall mobility under subswitching conditions (measured E field $< \frac{1}{3}E_C$) can be quantitatively reflected by the Rayleigh parameter α [12,13]. The Rayleigh analysis is carried out on both poled and unpoled PIN-PMN-0.27PT:Mn single crystals. For the poled samples, the Rayleigh behaviors of both the longitudinal dielectric constant ε_{33} (the measured field along $E_{||}$, parallel to the poling direction $[001]_C$) and the transverse constant ε_{11} (the measured field along $E_{\perp}$, perpendicular to $[001]_C$, e.g., along $[010]_C$ or $[100]_C$) are measured to estimate the domain-wall mobility under $E_{||}$ and $E_{\perp}$ [8]. All of the parameters are compared to those of the undoped PIN-PMN-0.27PT single crystal to quantify the clamped effect in Mn-doped crystal. Figure 1 shows the Rayleigh behavior of ε_r, ε_{33}, and ε_{11} for the two crystals. The measured and calculated P-E hysteresis loops in each mode are also shown in Fig. 1, and the α values of ε_r, ε_{11}, and ε_{33} are listed in Table I. For the PIN-PMN-0.27PT single crystal, ε_r and ε_{33} closely follow the Rayleigh law: the dielectric constant increases linearly with E_0, and the measured and calculated P-E loops coincided well with each other [Figs. 1(a) and 1(b)]. The Rayleigh parameter α is 1214 cm kV^{-1} for ε_r and only 119 cm kV^{-1} for ε_{33}. The Raleigh behavior of the transverse dielectric constant ε_{11} is significantly different from that of ε_r and ε_{33}. ε_{11} increases nonlinearly with E_0 above 0.5 kV cm^{-1} [Fig. 1(c)]. Such a

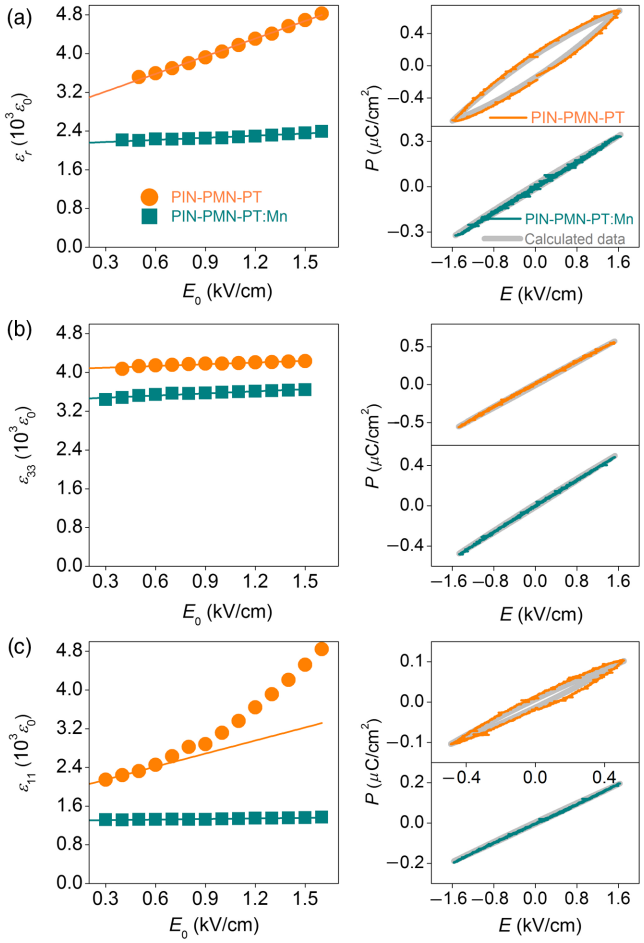

FIG. 1. Rayleigh behavior for ε_r, ε_{33}, and ε_{11}, including the dielectric constant as a function of amplitude E_0, measured and calculated P-E hysteresis loops for PIN-PMN-0.27PT and PIN-PMN-0.27PT:Mn. (a) ε_r for an unpoled sample. (b) ε_{33} for a poled sample. (c) ε_{11} for a poled sample.

superlinear increase of dielectric constant has also been observed in $Pb(Zr, Ti)O_3$ ceramics when the amplitude E_0 is above 4 kV/cm [14]. It was explained that when E_0 is above a critical value, domain nucleation occurs, resulting in an increase of domain-wall density. Therefore, the extrinsic contributions from domain-wall motion are enhanced correspondingly, and a superlinear increase of dielectric constant with E_0 can be observed [14–16]. From Fig. 1(c), we know that domain nucleations easily occur in PIN-PMN-0.27PT under $E_\perp$.

The linear fitting of ε_{11} in the low-electric-field region exhibits a high α value of 898 m kV^{-1}. It can be concluded that domain walls are highly movable in the unpoled PIN-PMN-0.27PT crystal. It can be concluded that, in the $[001]_C$ poled state with the $4R$ domain configuration, domain-wall motion is significantly clamped under the parallel field $E_{||}$ but easily excited under the perpendicular field $E_\perp$. The four P_S directions in the poled sample are energetically equivalent with respect to $E_{||}$ [8]. Hence, the switching of these four kinds of P_S places constraints one on another, which significantly inhibits the domain-wall mobility, resulting in a significant decrease of α under $E_{||}$. However, the four P_S directions are not equivalent with respect to $E_\perp$ [8]. Therefore, the components of P_S are less restricted by each other during switching under $E_\perp$, leading to a high level of domain-wall mobility and easier reverse domain nucleation.

For the PIN-PMN-0.27PT:Mn single crystal, the three dielectric constants, ε_r, ε_{33}, and ε_{11}, all closely follow the Rayleigh law. The Rayleigh parameter α of ε_r is 146 cm kV^{-1}, which is 1 order of magnitude lower than that of PIN-PMN-0.27PT (1214 cm kV^{-1}). For the longitudinal dielectric constant ε_{33}, α is 145 cm kV^{-1}, comparable to that of ε_{33} for PIN-PMN-0.27PT. The transverse constant ε_{11} of PIN-PMN-0.27PT:Mn demonstrates an extremely low α value of 39 cm kV^{-1}, much lower than that of PIN-PMN-0.27PT. Comparing the three α values of the two crystals, we can conclude that domain-wall mobility is anisotropically pinned after the introduction of Mn: it is significantly suppressed under $E_\perp$ but less affected under $E_{||}$.

B. Quantitative determination of polarization rotation

The intrinsic properties are related to the P_S rotation under an external E field [17–20]. In Table I, we list the intrinsic dielectric contributions ε_{in} of ε_r, ε_{33}, and ε_{11} for the two crystals to obtain the information of P_S rotation in different modes. The ratios of ε_{in} for PIN-PMN-0.27PT:Mn to PIN-PMN-0.27PT are also calculated and listed in Table I. We can observe that the ε_{in} values of PIN-PMN-0.27PT:Mn

TABLE I. ε_{in} and α values of ε_r, ε_{33}, and ε_{11} for PIN-PMN-0.27PT and PIN-PMN-0.27PT:Mn single crystals. Ratios of ε_{in} between the two crystals are also listed.

	Parameters	ε_{in} (ε_0)	α (cm kV^{-1})	Ratio of ε_{in}
ε_r	PIN-PMN-0.27PT	2854 ± 24	1214 ± 22	74.6% ± 1.1%
	PIN-PMN-0.27PT:Mn	2129 ± 13	146 ± 12	
ε_{33}	PIN-PMN-0.27PT	4062 ± 12	119 ± 12	84.5% ± 0.6%
	PIN-PMN-0.27PT:Mn	3435 ± 13	145 ± 14	
ε_{11}	PIN-PMN-0.27PT	1877 ± 10	898 ± 24	69.1% ± 0.6%
	PIN-PMN-0.27PT:Mn	1298 ± 4	39 ± 3	

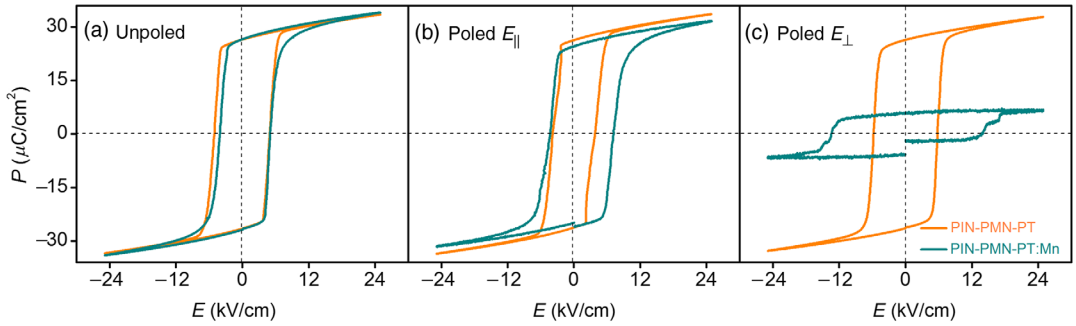

FIG. 2. *P-E* hysteresis loops for $[001]_C$-oriented PIN-PMN-0.27PT:Mn and PIN-PMN-0.27PT. (a) Unpoled. (b) Poled samples under $E_{||}$. (c) Poled samples under $E_{\perp}$.

in the three cases are all lower than the corresponding values of PIN-PMN-0.27PT, indicating that the P_S rotation is suppressed in acceptor-doped ferroelectrics. For the unpoled sample, ε_{in} of PIN-PMN-0.27PT:Mn is 74.6% that of PIN-PMN-0.27PT. For the poled sample, the ratio for ε_{33} is 84.5%, whereas it is only 69.1% for ε_{11}. These results indicate that polarization rotation is also anisotropically inhibited by Mn doping: it is more severe under $E_{\perp}$ than under $E_{||}$.

C. Polarization switching under a high *E* field

In order to further understand domain dynamics under a high E field ($>2E_C$), the *P-E* hysteresis loops for both unpoled and poled PIN-PMN-0.27PT:Mn and PIN-PMN-0.27PT single crystals are measured. For poled samples, two kinds of *P-E* loops are obtained with the measured E field along $E_{||}$ and $E_{\perp}$. The results are shown in Fig. 2, and the coercive field E_C and remnant polarization P_r are listed in Table II. For the PIN-PMN-0.27PT crystal, P_r values of the three modes are similar, i.e., approximately 26.5 μC cm^{-2}. The coercive field E_C under $E_{||}$ is lower than that of the unpoled sample, whereas E_C under $E_{\perp}$ is slightly higher than that of the unpoled sample. It can be concluded that, without acceptor ions, P_S can be completely switched in all the three cases, but the polarization switching is easier under $E_{||}$ than under $E_{\perp}$ owing to the constraints among coexisting domains. For the PIN-PMN-0.27PT:Mn crystal, P_r under $E_{||}$ (approximately 24.5 μC cm^{-2}) is comparable to that of the unpoled sample (26.8 μC cm^{-2}), but the value under $E_{\perp}$ (6.05 μC cm^{-2}) is much smaller, i.e., only approximately 22% of the unpoled sample. The coercive field in the poled PIN-PMN-0.27PT:Mn crystal is also strongly anisotropic: 5.80 kV cm^{-1} under $E_{||}$ and 13.41 kV cm^{-1} under $E_{\perp}$, both of which are higher than that of the unpoled sample (4.40 kV cm^{-1}).

IV. DISCUSSION

A. Formation of internal bias and its pinning effect

To determine the valence state of Mn in PIN-PMN-0.27PT:Mn, an electron spin resonance (ESR) measurement is carried out, and the results are shown in Fig. 3(a). As can be seen from the figure, Mn^{2+} is dominant in this crystal, similar to the situation in Mn-doped PMN-PT, $Pb(Zn_{1/3}Nb_{2/3})O_3$–$PbTiO_3$, and $0.92(Na_{0.5}Bi_{0.5})TiO_3$-$0.08(K_{0.5}Bi_{0.5})TiO_3$ single crystals [21–23]. Mn^{3+} is not detectable owing to its even number of $3d$ electrons.

Mn^{2+} occupies Ti sites owing to a similar ionic radius. In order to maintain the charge balance, oxygen vacancies $V_O^{\bullet\bullet}$ are created near Mn^{2+} [22]. Consequently, Mn^{2+}-$V_O^{\bullet\bullet}$ defect dipoles (P_d's) are formed [Fig. 3(b)]. It can be inferred that most of the Mn^{2+}-$V_O^{\bullet\bullet}$ defect dipoles are along the six $\langle 001\rangle_C$ directions [Fig. 3(c)]. The defect dipoles realign themselves along the three preferential directions closest to P_S in a given domain to minimize the total electrostatic energy [Fig. 3(d)] [24,25], resulting in an internal bias (E_i). In each domain, E_i should be antiparallel to P_S. In an unpoled sample, eight allowed domains are distributed randomly, and hence there are no preferential directions for E_i. These P_d's may realign under an external E field via $V_O^{\bullet\bullet}$ hopping [26,27]. During the poling process, some of the Mn^{2+}-$V_O^{\bullet\bullet}$ dipoles adjust their orientations to the

TABLE II. Coercive field E_C, internal bias E_i, and remnant polarization P_r of the three measured modes.

Materials		E_C (kV cm^{-1})	E_i (kV cm^{-1})	P_r (μC cm^{-2})
Unpoled	PIN-PMN-0.27PT	4.84 ± 0.12	0.05 ± 0.02	26.5 ± 0.9
	PIN-PMN-0.27PT:Mn	4.40 ± 0.33	0.50 ± 0.02	26.8 ± 0.4
Poled ($E_{||}$)	PIN-PMN-0.27PT	3.83 ± 0.26	0.01 ± 0.01	26.3 ± 0.5
	PIN-PMN-0.27PT:Mn	5.80 ± 0.25	1.44 ± 0.03	24.5 ± 1.7
Poled ($E_{\perp}$)	PIN-PMN-0.27PT	5.77 ± 0.13	0.00 ± 0.01	26.5 ± 0.1
	PIN-PMN-0.27PT:Mn	13.41 ± 2.11	0.12 ± 0.06	6.05 ± 1.16

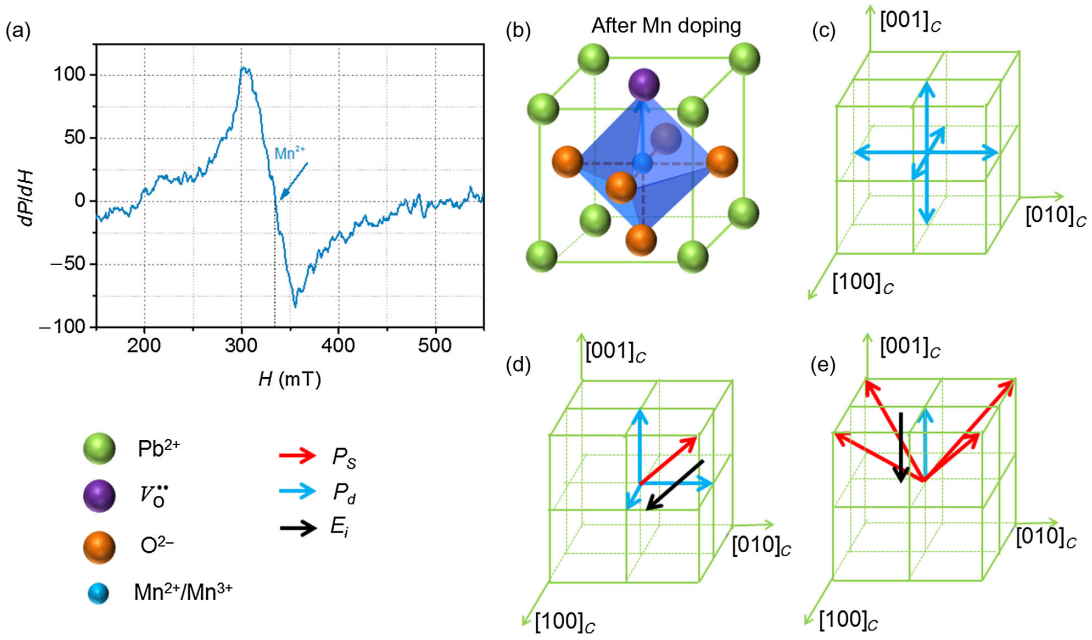

FIG. 3. (a) ESR spectrum of PIN-PMN-0.27PT:Mn crystal. (b) Formation of Mn^{2+}-$V_O^{\bullet\bullet}$ defect dipoles P_d in the perovskite ABO_3 structure. (c) Possible directions of P_d. (d) P_d directions and internal bias E_i with respect to P_S in a given domain. (e) Directions of P_S, P_d, and E_i in $[001]_C$ poled samples.

energetically preferred E-field direction $[001]_C$. Consequently, a macroscopic bias field E_i along $[00\bar{1}]_C$ is formed, as shown in Fig. 3(e). Based on the P-E loops in Fig. 2, we can experimentally determine the strength and direction of the internal bias in a $[001]_C$ poled sample, as listed in Table II. E_i of PIN-PMN-0.27PT in all three cases can be neglected. For the $[001]_C$ poled PIN-PMN-0.27PT:Mn crystal, E_i under $E_{||}$ is 1.44 kV cm^{-1} along $[00\bar{1}]_C$, whereas under $E_\perp$, it is only 0.12 kV cm^{-1}, which is negligible. The experimental results are consistent with the above analysis. Notably, the relaxation time of P_d is on the order of 10^5 s at room temperature [28], which is much longer than that of P_S (10^{-6}–10^{-5} s). Moreover, the activation energy of the $V_O^{\bullet\bullet}$ hopping (approximately 1 eV) is much higher than the activation energy of the domain walls (approximately 0.1 eV) [29–31]. Therefore, only a small fraction of the Mn^{2+}-$V_O^{\bullet\bullet}$ dipoles are switched during poling. The detailed dynamics of P_d under the external E field are available in Sec. C of the Supplemental Material [8].

Furthermore, we discuss the pinning effect of the internal bias. When $E_{||}$ is applied, E_i enhances or counters the applied E field because they are parallel or antiparallel to each other; thus, domain-wall motion and P_S rotation may be affected. As is evident from Fig. 1 and Table I, poled PIN-PMN-PT and PIN-PMN-PT:Mn exhibit similar α values under $E_{||}$, indicating that E_i does not significantly clamp the domain-wall motion in this mode. The low domain-wall motion is mostly due to the constraints of the 4R domain structure, rather than the internal bias. When P_S switches under a high $E_{||}$ field [Fig. 2(b)], a part of $E_{||}$ is counteracted by E_i, leading to an increase in the coercive field E_C. Notably, E_C under $E_{||}$ (5.80 kV cm^{-1}) is 1.40 kV cm^{-1} higher than that of the undoped sample (4.40 kV cm^{-1}). This deviation is very close to E_i (1.44 kV cm^{-1}), further confirming that the increased difficulty in P_S switching is due to the inhibition of internal bias. The activation energy E_a of the P_S switching under $E_{||}$ is determined to be 0.230 and 0.008 eV for PIN-PMN-0.27PT:Mn and PIN-PMN-0.27PT, respectively, as can be seen in Fig. 4(a) (detailed information on the activation energy E_a can be found in Sec. D of the Supplemental Material [8]). Hence, the internal bias effectively inhibits P_S switching by enhancing the activation energy [31–33]. Under $E_\perp$, the domain-wall mobility in PIN-PMN-0.27PT:Mn is significantly clamped (see Fig. 1 and Table I). The extremely low P_r value and high E_C value [see Fig. 2(c) and Table II] also reveal a strong pinning effect on the P_S switching. This pinning effect does not originate from the internal bias, for the following reasons: First, E_i and $E_\perp$ are perpendicular to each other; thus, E_i may not significantly affect the domain-wall movement and P_S switching under $E_\perp$. Second, E_i is only 1.44 kV cm^{-1}. Its inhibition effect, if any, should be easily canceled by an external $E_\perp$ field of 25 kV cm^{-1}. Therefore, we conclude that there are other factors that strongly clamp the domain-wall motion and suppress P_S switching under $E_\perp$.

Subsequently, the inhibition of E_i on P_S rotation is discussed. In the PIN-PMN-0.27PT:Mn crystal, an additional force moment produced by E_i is applied on the P_S vectors, which restricts their deviation from the equilibrium position when an ac E field is applied, resulting in the

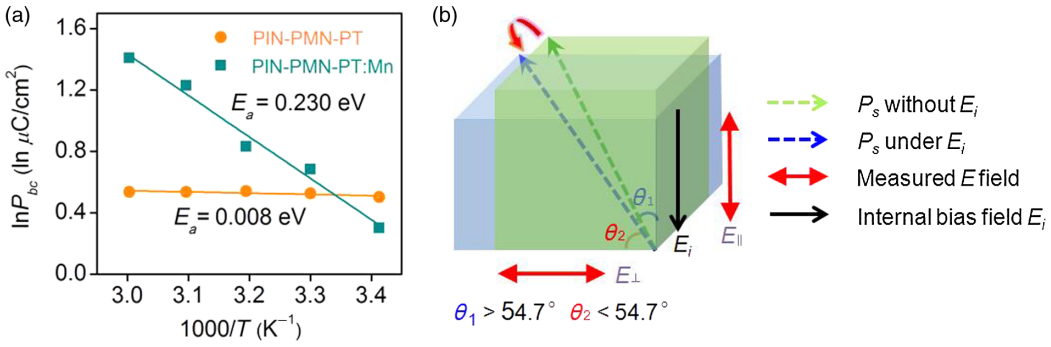

FIG. 4. (a) Plot of $\ln(P_{bc})$ versus inverse temperature, from which the activation energy E_a of the P_S switching under $E_{||}$ can be determined. (b) Schematic representation of the influence of the internal bias on the P_S rotation.

suppression of the P_S rotation. The anisotropic pinning effect on P_S rotation is due to the directional characteristic of E_i. Under the torque of E_i, the four upward P_S's rotate downward by a small angle, as shown in Fig. 4(b). Hence, the angle θ_1 between P_S and $E_{||}$ becomes slightly larger than 54.7°, whereas the angle θ_2 between P_S and $E_\perp$ becomes slightly smaller than 54.7° [Fig. 4(b)].

When $E_{||}$ is applied, P_S rotates under the torque $\overrightarrow{M_{33}}$:

$$\overrightarrow{M_{33}} = \overrightarrow{P_S} \times \overrightarrow{E_{||}}. \quad (1)$$

The magnitude of this torque can be written as

$$M_{33} = P_S E_{||} \sin\theta_1. \quad (2)$$

When $E_\perp$ is applied, P_S rotates under the external torque $\overrightarrow{M_{11}}$,

$$\overrightarrow{M_{11}} = \overrightarrow{P_S} \times \overrightarrow{E_\perp}, \quad (3)$$

and the magnitude is

$$M_{11} = P_S E_\perp \sin\theta_2. \quad (4)$$

θ_1 is slightly larger than θ_2, and hence M_{33} should be larger than M_{11} when the magnitudes of the external field are the same. Consequently, P_S rotates easier under $E_{||}$ than under $E_\perp$.

B. Formation of charged domain walls and their pinning effect

Another difference between the two crystals is that there are numerous charged defects in the Mn-doped crystal owing to the aliovalent doping. It has been reported that charged domain walls have lower energy than neutral domain walls in a ferroelectric with a high amount of charged defects [34]. Thus, charged domain walls can be easily formed in PIN-PMN-PT:Mn single crystals. The charged and neutral domain walls for the 4R domain structure are illustrated in Figs. 5(a)–5(d). It is evident that, when observed on the $(001)_C$ surface, the charged 109° domain wall should be along $[110]_C$ (abbreviated as $S4$) or $[\bar{1}10]_C$ ($S3$), whereas the charged 71° domain wall is along $[100]_C$ ($S1$) or $[010]_C$ ($S2$), as shown in Figs. 5(a), 5(b), and 5(f). For the neutral domain walls, 71° is along $[100]_C$ ($S1$) or $[010]_C$ ($S2$), whereas 109° cannot be observed, as shown in Figs. 5(c), 5(d), and 5(f). The charged 109° domain and the neutral 71° domain are preferred over the 71° charged domain and the neutral 109° domain owing to their lower elastic energy.

The domain structures in the two crystals are observed using polarizing light microscopy (PLM) and piezoresponse force microscopy (PFM). Domain structures of six different regions on each sample are observed by PLM; results are shown in Fig. S6 of the Supplemental Material [8]. As can be seen, in the PIN-PMN-PT crystal, most domain walls are neutral 71° domains (regions A, E, F, G, and H), and only a small amount of the 109° charged domain can be observed at the edge of the sample (region B). The formation of these charged domain walls is ascribed to the special stress state at the edge of the sample, whereas, for most of the interior part, neutral domain walls are preferred. For the PIN-PMN-0.27PT:Mn crystal, charged 109° domains walls ($S3$ and $S4$) can be easily observed both at the edge (regions C and J) and in the interior regions (regions D, I, K, and L). We further observe the domain structures by PFM, and the results are shown in Figs. 5(i), 5(j), 5(l) and 5(m). As can be seen, 109° charged domain walls ($S3$) can be observed in PIN-PMN-0.27PT:Mn single crystal, and natural 71° domain walls ($S1$) are observed in PIN-PMN-0.27PT crystal. Based on the experimental results, we know that charged domain walls can be easily formed in PIN-PMN-0.27PT:Mn single crystal.

Furthermore, we consider the clamp effect of the charged domain walls. Immediately after the formation of a head-to-head charged domain wall, it neutralizes partially the negative charge of Mn ions, and the positively charged ions of oxygen vacancies $V_O^{\bullet\bullet}$ are repelled away from the head-to-head charged domain walls and gradually migrate toward tail-to-tail domain walls. As a result, in a sufficiently aged sample, $V_O^{\bullet\bullet}$ vacancies concentrate at the tail-to-tail charged domain walls, while Mn ions are left at the head-to-head charged domain walls, as shown in Fig. 5(l). On the other hand, the concentrated charged defects, in turn, strongly pin the domain-wall motion via electrostatic interactions. The electrostatic force is too strong to be completely canceled by an external E field. As evident from

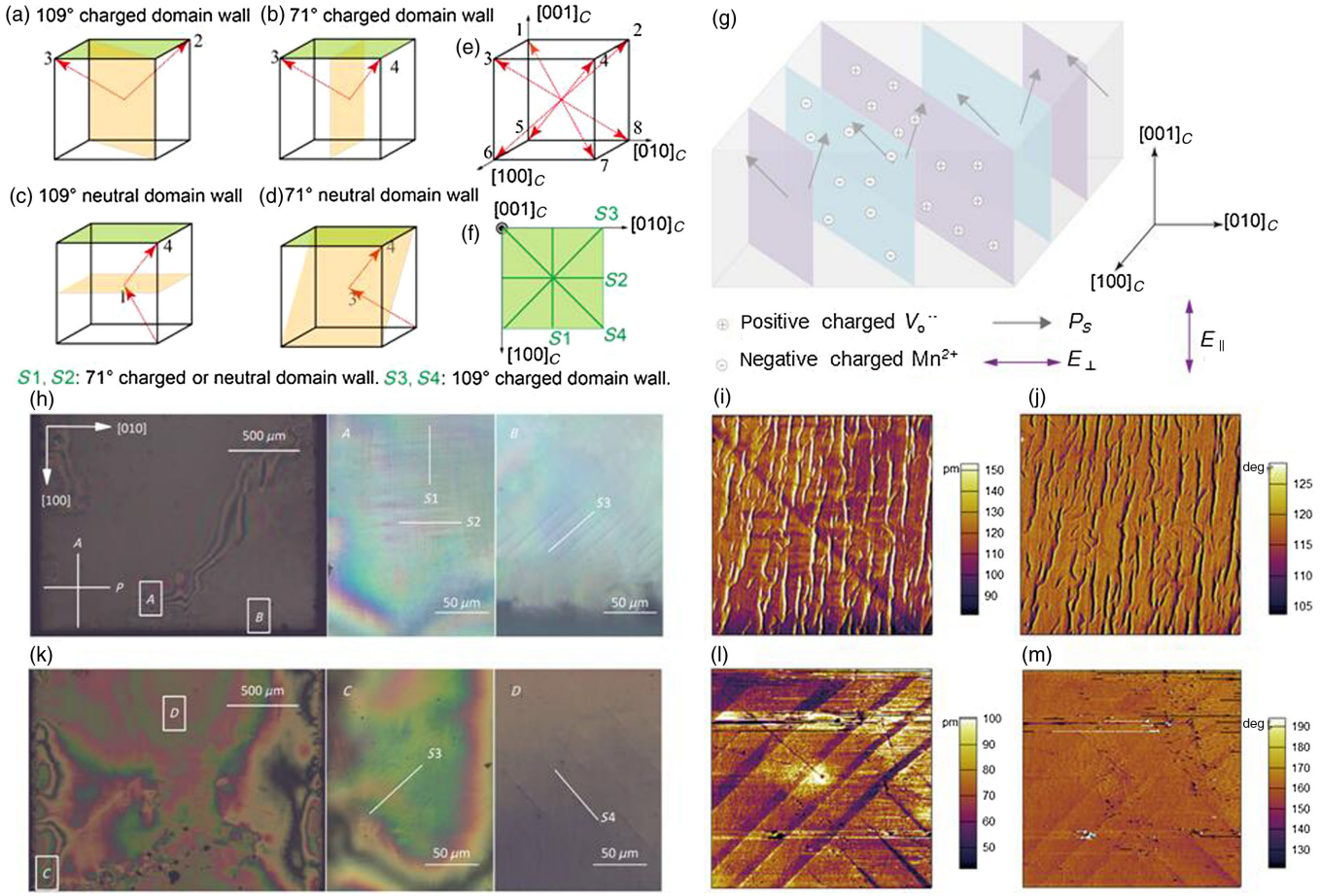

FIG. 5. Domain structure of the two crystals. (a),(b) Schematics of charged 109° and 71° domain walls, respectively. (c),(d) are 109° and 71° neutral domain walls, respectively. (e) P_S directions in a perovskite structure in the R phase. (f) Possible directions of domain walls when observed on the $(001)_C$ surface. (h),(k) Domain structures observed by PLM for PIN-PMN-0.27PT and PIN-PMN-0.27PT:Mn single crystals. (i),(j) PFM amplitude and phase images of PIN-PMN-0.27PT. (l),(m) Amplitude and phase images of PIN-PMN-0.27PT:Mn. (g) Schematic of charged domain walls with respect to $E_\perp$ and $E_{||}$ in a PIN-PMN-0.27PT:Mn single crystal.

Fig. 5(g), the pinning effects of charged domain walls under $E_\perp$ and $E_{||}$ are different. When $E_\perp$ is applied, it is difficult for the P_S vectors to switch, for the charge balance at the domain wall may be destroyed. Therefore, the inhibition effect in this situation is extremely strong, which is consistent with our experimental results [see Figs. 1(c) and 2(c)]. By contrast, the charge balance at the domain wall is maintained when P_S vectors switch under $E_{||}$. Thus, P_S vectors switch and the domain-wall movement is not significantly inhibited in this case, which is consistent with our experimental results in Figs. 1(b) and 2(b). It should be noted that the formation of charged domain walls depends on many factors, such as the stress distribution and the concentration dispersion of Mn ions. Therefore, the density and the amount of the charged domain walls vary greatly between samples and in different regions of a given sample. The pinning effect under $E_\perp$ also reveals such a difference [8].

The rotation of P_S vectors in the vicinity of the charged domain walls may also be suppressed. However, the volume fraction of such P_S vectors is small because most of them are inside the domain matrix away from the domain walls. Hence, the inhibition of P_S rotation is mainly ascribed to the internal bias.

C. Enhancement of the mechanical quality factor Q_m

The mechanical loss A can be divided into the intrinsic part A_{in} and the extrinsic part A_{ex}:

$$A = A_{\text{in}} + A_{\text{ex}}; \tag{5}$$

thus, the mechanical quality factor Q_m can be expressed as

$$Q_m = \frac{1}{A_{\text{in}} + A_{\text{ex}}}. \tag{6}$$

The enhancement of Q_m might be attributed to the decrease of A_{in} (the restricted P_S rotation), the decrease of A_{ex} (the clamped domain-wall motion), or both. It is necessary to quantitatively separate A_{in} and A_{ex} to further investigate the influence of Mn doping on the two types of contributions. Notably, A_{in} and A_{ex} may vary for different

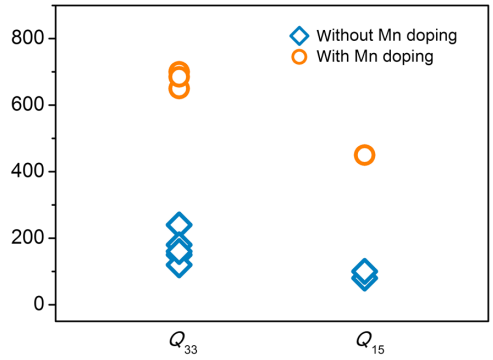

FIG. 6. Mechanical quality factors Q_{33} and Q_{15} for the $[001]_C$ poled relaxor-based ferroelectric single crystal with (circles) and without (diamonds) Mn doping. Data here include Q_{33} and Q_{15} values of PIN-PMN-PT [7,35], PMN-PT [36–38] and PIN-PMN-PT:Mn [9,10,39].

vibration modes. For the longitudinal mechanical quality factor Q_{33}, the measured field is along $E_{||}$, whereas for the shear factor Q_{15}, the measured field is $E_{\perp}$. There are large differences in A_{ex} in the two modes owing to the large disparity of domain-wall mobility under $E_{||}$ and $E_{\perp}$. Figure 6 shows Q_{33} and Q_{15} in PIN-PMN-PT, PMN-PT, and PIN-PMN-PT:Mn single crystals with and without Mn doping in the $4R$ domain structure obtained in this work and in the literature. It can be observed that both factors are enhanced significantly after the introduction of Mn. The average enhancement of Q_{33} is approximately 320% (from approximately 160 to 680), whereas the increase of Q_{15} is approximately 400% (from 90 to 450).

The intrinsic mechanical loss A_{in} originates from the P_S rotation. The rotation of a P_S vector under the ac field $E_0 \cos \omega t$ (where ω is the angular frequency and E_0 is the amplitude) is given by

$$I\frac{d^2\beta}{dt^2} + \gamma\frac{d\beta}{dt} + K\beta = E_0 P_S \sin\theta \cos\omega t, \tag{7}$$

where β is the angular displacement from the equilibrium position at time t, I is the moment of inertia of P_S, γ is the damping moment factor during P_S rotation, K is the coefficient of restoring moment, θ is the angle between the field and P_S vector, and $E_0 P_S \sin\theta\cos\omega t$ is the torque caused by the measurement field. The intrinsic loss A_{in} can be expressed as

$$A_{in} = \frac{\pi\gamma\omega {E_0}^2 {P_S}^2 \sin^2\theta}{\sqrt{\gamma^2\omega^2 + (K - I\omega^2)^2}}. \tag{8}$$

The derivations of Eqs. (7) and (8) can be found in the Supplemental Material [8]. P_S and I are affected only slightly by Mn doping [see Figs. 2(a) and 2(b)], but K and γ are significantly influenced by the formation of internal bias E_i, resulting in the reduction of A_{in}. Furthermore, according to Eq. (8), the direction of P_S, internal bias E_i, and the measured E field also significantly influence A_{in}. Therefore, A_{in} varies significantly in different domain structures. The extrinsic mechanical loss A_{ex} is closely related to the domain-wall mobility, i.e., proportional to the Rayleigh parameter α [15]. According to the α values in Fig. 1 and Table I, it is estimated that A_{ex} exhibits a slight change in the longitudinal mode but is reduced by 96% in the shear mode after Mn doping.

In the longitudinal mode, both crystals exhibit low domain-wall mobility. According to this work and previous reports in the literature, in the crystals, which are far away from the MPB, the extrinsic contributions to the longitudinal properties ε_{33} and d_{33} are very low (<5%) [9,40]. It is reasonable to neglect the extrinsic mechanical loss in the longitudinal mode. Based on Fig. 6, we can obtain the following relationship:

$$\frac{420\%}{A_{in33}} = \frac{1}{A^*_{in33}}, \tag{9}$$

where A_{in33} and A^*_{in33} are the longitudinal intrinsic mechanical loss for crystals without and with Mn doping, respectively. The ratio of the two intrinsic losses is $A_{in33}/A^*_{in33} = 4.2$. The enhancement of Q_{33} originates mainly from the reduction of A_{in}—more specifically, from the restriction of P_S rotation. It is experimentally confirmed that, in the Mn-doped PMN-PT–based crystals, the enhancement of Q_{33} is approximately 20%–100%, 100%, and 320%, respectively, for the $1R$, $2R$, and $4R$ domain configurations [10]. The extremely different enhancements are ascribed to the different pinning strengths on the P_S rotation in various domain configurations. These results further confirm that the enhancement of Q_{33} originates mainly from the reduction of the intrinsic A_{in}, but not from the extrinsic A_{ex}.

During the measurement of Q_{15}, high domain-wall mobility is excited by $E_{\perp}$ in crystals without Mn, and both intrinsic and extrinsic contributions should be considered. A relationship similar to Eq. (9) may be used:

$$\frac{500\%}{A_{in15} + A_{ex15}} = \frac{1}{A^*_{in15} + A^*_{ex15}}, \tag{10}$$

where A_{in15} and A_{ex15} are the intrinsic and extrinsic mechanical losses for the crystal without Mn, respectively, and A^*_{in15} and A^*_{ex15} are the corresponding values for Mn-doped crystals, respectively. According to the α values in Fig. 1 and Table I, A^*_{ex15} should be only 4% of A_{ex15}. For the $4R$ domain structure, the angles between $E_{||}$ and P_S and between $E_{\perp}$ and P_S are both approximately 54.7°. According to Eq. (8), the reduction of A_{in15} is similar to A_{in33}; therefore,

$$\frac{A_{in15}}{A^*_{in15}} \approx \frac{A_{in33}}{A^*_{in33}} = 4.2. \tag{11}$$

Combining Eqs. (10) and (11), we obtain

$$\frac{A_{\text{in15}}}{A_{\text{ex15}}} = 4.2 \tag{12}$$

and

$$\frac{A^*_{\text{in15}}}{A^*_{\text{ex15}}} = 25. \tag{13}$$

In the shear mode, the extrinsic part contributes 19% of the total mechanical loss in the PIN-PMN-PT single crystal. After the introduction of Mn, the extrinsic part is reduced significantly to a negligible level. Hence, the enhancement of the shear factor Q_{15} in the Mn-doped crystal is attributed to both the restricted P_S rotation and the clamped domain-wall motion.

V. SUMMARY AND CONCLUSIONS

In this paper, we systematically study different inhibition effects in accepter-ion-doped relaxor-based PIN-PMN-0.27PT ferroelectric single crystals. The domain-wall mobility and P_S rotation of PIN-PMN-0.27PT:Mn single crystals are quantitatively investigated. Our results indicated that P_S rotations are anisotropically inhibited by the internal bias. The lower domain-wall mobility under $E_{||}$ is ascribed mainly to the mutual domain pinning of the $4R$ domain structure, not to the internal bias. However, charged defects bounded to the charged domain walls strongly clamp the domain-wall motion and the P_S switching under $E_{\perp}$, resulting in an extremely low Rayleigh parameter (39 cm kV^{-1}), low remnant polarization (6.05 $\mu\text{C cm}^{-2}$), and a high coercive field (13.41 kV cm^{-1}). We also successfully separate the intrinsic and extrinsic parts of mechanical quality factors Q_{33} and Q_{15} and observe that the enhanced Q_{33} originates mainly from the restricted polarization rotation, whereas the improvement of Q_{15} originates from both the restricted polarization rotation and the clamped domain-wall motion. Our results clarify the interaction between acceptor ions and domain dynamics in accepter-doped Pb-based relaxor single crystals, which can provide general guidance for the optimization of functional properties of ferroelectric materials and the control of mechanical Q_m values using different doping strategies.

ACKNOWLEDGMENTS

This work was supported by the National Key Basic Research Program of China (Grant No. 2013CB632900), the National Natural Science Foundation of China (Grants No. 51572055, No. 11372002, and No. 51602080), and the Natural Science Foundation of Heilongjiang Province (Grant No. E2017031).

[1] S. Zhang, J. Luo, W. Hackenberger, and T. R. Shrout, Characterization of $Pb(In_{1/2}Nb_{1/2})O_3$–$Pb(Mg_{1/3}Nb_{2/3})O_3$–$PbTiO_3$ ferroelectric crystal with enhanced phase transition temperatures, J. Appl. Phys. **104**, 064106 (2008).

[2] F. Li, S. Zhang, D. Lin, J. Luo, Z. Xu, X. Wei, and T. R. Shrout, Electromechanical properties of $Pb(In_{1/2}Nb_{1/2})O_3 - Pb(Mg_{1/3}Nb_{2/3})O_3 - PbTiO_3$ single crystals, J. Appl. Phys. **109**, 014108 (2011).

[3] L. Zheng, X. Lu, H. Shang, Z. Xi, R. Wang, J. Wang, and W. Cao, Hysteretic phase transition sequence in $0.67Pb(Mg_{1/3}Nb_{2/3})O_3 - 0.33PbTiO_3$ single crystal driven by electric field and temperature, Phys. Rev. B **91**, 184105 (2015).

[4] L. Zheng, Y. Jing, X. Lu, R. Wang, G. Liu, W. Lü, and W. Cao, Temperature and electric-field induced phase transitions, and full tensor properties of $[011]_C$-poled domain-engineered tetragonal $0.63Pb(Mg_{1/3}Nb_{2/3}) - 0.37PbTiO_3$ single crystals, Phys. Rev. B **93**, 094104 (2016).

[5] S. Zhang and F. Li, High performance ferroelectric relaxor-$PbTiO_3$ single crystals: Status and perspective, J. Appl. Phys. **111**, 031301 (2012).

[6] E. Sun, W. Cao, W. Jiang, and P. Han, Complete set of material properties of single domain $0.24Pb(In_{1/2}Nb_{1/2})O_3 - 0.49Pb(Mg_{1/3}Nb_{2/3})O_3 - 0.27PbTiO_3$ single crystal and the orientation effects, Appl. Phys. Lett. **99**, 032901 (2011).

[7] G. Liu, S. Zhang, W. Jiang, and W. Cao, Losses in ferroelectric materials, Mater. Sci. Eng. R **89**, 1 (2015).

[8] See Supplemental Material at http://link.aps.org/supplemental/10.1103/PhysRevApplied.9.064028 for further details of P_S, domain dynamics, the Rayleigh law, internal bias, dynamics of defect dipoles, activation energy of P_S switching, charged domain walls and their pinning effect, and intrinsic mechanical loss.

[9] L. Zheng, R. Sahul, S. Zhang, W. Jiang, S. Li, and W. Cao, Orientation dependence of piezoelectric properties and mechanical quality factors of $0.27Pb(In_{1/2}Nb_{1/2})O_3 - 0.46Pb\ (Mg_{1/3}Nb_{2/3})O_3 - 0.27PbTiO_3$: Mn single crystals, J. Appl. Phys. **114**, 104105 (2013).

[10] N. Luo, S. Zhang, Q. Li, Q. Yan, Y. Zhang, T. Ansell, and T. R. Shrout, Crystallographic dependence of internal bias in domain engineered Mn-doped relaxor-$PbTiO_3$ single crystals, J. Mater. Chem. C **4**, 4568 (2016).

[11] L. Yang, L. Zheng, Y. Jing, S. Li, X. Lu, W. Lü, and R. Zhang, Temperature dependence of intrinsic and extrinsic dielectric contributions in $0.27Pb(In_{1/2}Nb_{1/2})O_3 - 0.46Pb(Mg_{1/3}Nb_{2/3})O_3 - 0.27PbTiO_3$ single crystals, Phys. Status Solidi B **254**, 1700029 (2017).

[12] M. Davis, D. Damjanovic, and N. Setter, Temperature dependence of the direct piezoelectric effect in relaxor-ferroelectric single crystals: Intrinsic and extrinsic contributions, J. Appl. Phys. **100**, 084103 (2006).

[13] M. Davis, D. Damjanovic, and N. Setter, Direct piezoelectric effect in relaxor-ferroelectric single crystals, J. Appl. Phys. **95**, 5679 (2004).

[14] D. A. Hall and P. J. Stevenson, High field dielectric behavior of ferroelectric ceramics, Ferroelectrics **228**, 139 (1999).

[15] R. E. Eitel, T. R. Shrout, and C. A. Randall, Nonlinear contributions to the dielectric permittivity and converse piezoelectric coefficient in piezoelectric ceramics, J. Appl. Phys. **99**, 124110 (2006).

[16] T. Leist, T. Granzow, W. Jo, and J. Rodel, Effect of tetragonal distortion on ferroelectric domain switching: A case study on La-doped $BiFeO_3 - PbTiO_3$ ceramics, J. Appl. Phys. **108**, 014103 (2010).

[17] F. Li, S. Zhang, Z. Xu, X. Wei, and T. R. Shrout, Critical property in relaxor-$PbTiO_3$ single crystals—Shear piezoelectric response, Adv. Funct. Mater. **21**, 2118 (2011).

[18] D. Damjanovic, Contributions to the piezoelectric effect in ferroelectric single crystals and ceramics, J. Am. Ceram. Soc. **88**, 2663 (2005).

[19] M. Davis, M. Budimir, D. Damjanovic, and N. Setter, Rotator and extender ferroelectrics: Importance of the shear coefficient to the piezoelectric properties of domain-engineered crystals and ceramics, J. Appl. Phys. **101**, 054112 (2007).

[20] L. Zheng, X. Yi, S. Zhang, W. Jiang, B. Yang, R. Zhang, and W. Cao, Complete set of material constants of $0.95(Na_{0.5}Bi_{0.5})TiO_3 - 0.05BaTiO_3$ lead-free piezoelectric single crystal and the delineation of extrinsic contributions, Appl. Phys. Lett. **103**, 122905 (2013).

[21] S. Zhang, L. Lebrun, C. A. Randall, and T. R. Shrout, Growth and electrical properties of (Mn, F) co-doped $0.92Pb(Zn_{1/3}Nb_{2/3})O_3 - 0.08PbTiO_3$ single crystal, J. Cryst. Growth **267**, 204 (2004).

[22] X. Li, X. Zhao, B. Ren, H. Luo, W. Ge, Z. Jiang, and S. Zhang, Microstructure and dielectric relaxation of dipolar defects in Mn-doped $(1-x)Pb(Mg_{1/3}Nb_{2/3})O_3 - xPbTiO_3$ single crystals, Scr. Mater. **69**, 377 (2013).

[23] H. Zhang, C. Chen, X. Zhao, H. Deng, L. Li, D. Lin, X. Li, B. Ren, H. Luo, and J. Yan, Enhanced ferroelectricity properties and thermal stability of nonstoichiometric $0.92(Na_{0.5}Bi_{0.5})TiO_3 - 0.08(K_{0.5}Bi_{0.5})TiO_3$ single crystals, Appl. Phys. Lett. **103**, 212906 (2013).

[24] X. Ren, Large electric-field-induced strain in ferroelectric crystals by point-defect-mediated reversible domain switching, Nat. Mater. **3**, 91 (2004).

[25] G. Du, R. Liang, L. Wang, K. Li, W. Zhang, G. Wang, and X. Dong, Large stable strain memory effect in poled Mn-doped $Pb(Mn_{1/3}Sb_{2/3})O_3 - Pb(Zr, Ti)O_3$ ceramics, Appl. Phys. Lett. **102**, 162907 (2013).

[26] M. S. Islam, Ionic transport in ABO_3 perovskite oxides: A computer modelling tour, J. Mater. Chem. **10**, 1027 (2000).

[27] R. Al-Hamadany, J. P. Goss, P. R. Briddon, S. A. Mojarad, M. Al-Hadidi, A. G. O'Neill, and M. J. Rayson, Oxygen vacancy migration in compressively strained $SrTiO_3$, J. Appl. Phys. **113**, 024108 (2013).

[28] W. L. Warren, K. Vanheusden, D. Dimos, G. E. Pike, and B. A. Tuttle, Oxygen vacancy motion in perovskite oxides, J. Am. Ceram. Soc. **79**, 536 (1996).

[29] J. S. Lee, S. Lee, and T. W. Noh, Resistive switching phenomena: A review of statistical physics approaches, Appl. Phys. Rev. **2**, 031303 (2015).

[30] S. Zhao, S. J. Zhang,W. Liu, N. J. Donnelly, Z. Xu, and C. A. Randall, Time dependent dc resistance degradation in lead-based perovskites: $0.7Pb(Mg_{1/3}Nb_{2/3})O_3 - 0.3PbTiO_3$, J. Appl. Phys. **105**, 053705 (2009).

[31] B. Ma, Z. Hu, S. Liu, M. Narayanan, and U. Balachandran, Temperature dependent polarization switching properties of ferroelectric $Pb_{0.92}La_{0.08}Zr_{0.52}Ti_{0.48}O_\delta$ films grown on nickel foils, Appl. Phys. Lett. **102**, 072901 (2013).

[32] G. Du, R. Liang, L. Wang, K. Li, W. Zhang, G. Wang, and X. Dong, Temperature dependent ferroelectric dynamic hysteresis properties of modified PMN-PZT relaxor ceramics, Phys. Status Solidi RRL **7**, 438 (2013).

[33] B. Wen, Y. Zhang, X. Liu, L. Ma, and X. Wang, Temperature-dependent ferroelectric hysteresis properties of modified lead zirconate titanate ceramics, J. Mater. Sci. **47**, 4299 (2012).

[34] Z. Li, H. Wu, and W. Cao, Piezoelectric response of charged non-180° domain walls in ferroelectric ceramics, J. Appl. Phys. **111**, 024106 (2012).

[35] S. Zhang, J. Luo, W. Hackenberger, N. P. Sherlock, R. J. Meyer, Jr., and T. R. Shrout, Electromechanical characterization of $Pb(In_{0.5}Nb_{0.5})O_3 - Pb(Mg_{1/3}Nb_{2/3})O_3 - PbTiO_3$ crystals as a function of crystallographic orientation and temperature, J. Appl. Phys. **105**, 104506 (2009).

[36] S. Zhang, F. Li, J. Luo, R. Sahul, and T. R. Shrout, Relaxor-$PbTiO_3$ single crystals for various applications, IEEE Trans. Ultrason. Ferroelectr. Freq. Control **60**, 1572 (2013).

[37] S. Zhang, N. P. Sherlock, R. J. Meyer, and T. R. Shrout, Crystallographic dependence of loss in domain engineered relaxor-PT single crystals, Appl. Phys. Lett. **94**, 162906 (2009).

[38] L. Luo, W. Li, Y. Zhu, and J. Wang, Growth and characteristics of Mn-doped PMN-PT single crystals, Solid State Commun. **149**, 978 (2009).

[39] X. Huo, S. Zhang, G. Liu, R. Zhang, J. Luo, R. Sahul, and T. R. Shrout, Complete set of elastic, dielectric, and piezoelectric constants of $[011]_C$ poled rhombohedral $Pb(In_{0.5}Nb_{0.5})O_3 - Pb(Mg_{1/3}Nb_{2/3})O_3 - PbTiO_3$:Mn single crystals, J. Appl. Phys. **113**, 074106 (2013).

[40] F. Li, S. Zhang, Z. Xu, X. Wei, J. Luo, and T. R. Shrout, Composition and phase dependence of the intrinsic and extrinsic piezoelectric activity of domain engineered $(1-x)Pb(Mg_{1/3}Nb_{2/3})O_3 - xPbTiO_3$ crystals, J. Appl. Phys. **108**, 034106 (2010).